BULLETIN OF THE POLISH ACADEMY OF SCIENCES
TECHNICAL SCIENCES, Vol. 70(5), 2022, Article number: e143105
DOI: 10.24425/bpasts.2022.143105

Thermal performance analysis of manned airships in a thermally variable environment

Hong SHI[1]*, Meinan LIU[1], Jiamin CHEN[1], and Yitao ZOU[2]

[1] College of Energy and Power Engineering, Jiangsu University of Science and Technology, China
[2] Key Laboratory of Aircraft Environment Control and Life Support, Nanjing University of Aeronautics and Astronautics, China

Abstract. The safety and reliability of the manned airship depend to a considerable extent on its thermal performance. In this paper, heat balance equations are developed and solved in the C++ programming language. The temperature variation of the enclosure, gasbag, and nacelles of the manned airship is investigated. In addition, the effects of season, latitude, and orientation on the thermal performance of the manned airship and the airship nacelle are investigated. The results show that: (1) The average temperature difference of the nacelle surface at the same time is 25 K, while the maximum temperature difference in the nacelle is 29 K during the day, (2) the temperature distribution in the nacelle is similar in spring and autumn, with maximum temperature between 306 K and 309 K. The maximum temperature in the nacelle is between 300 K and 303 K in winter while the maximum temperature in the nacelles is between 309 K and 315 K in summer, (3) as the flight position of the manned airship changes from 20°N to 60°N, the average nacelle temperature varies slightly by about 1 K. However, as the latitude increases, the high-temperature region shifts from the bottom of the nacelle to the side of the nacelle, and (4) the temperature distribution of the upper envelope of the airship varies considerably with orientation. However, the average temperature of the nacelle is less impacted by orientation. These results are useful for understanding the thermal performance of manned airships.

Key words: manned airship; thermal performance; nacelle; temperature difference; flight position.

1. INTRODUCTION

The manned airship can be used as a tourism, transportation, and rescue tool with obvious advantages such as long endurance, good safety performance, high strain capacity, and noise pollution, which can better meet the numerous needs of people flying in the air, thus attracting increased attention [1–3]. At present, several companies participate in the development of manned airships, including Lockheed Martin, Boeing, Worldwide Aeros Corp., Aero Vehicles Inc., Hybrid Air Vehicles Ltd. (HAV), and Voliris. ATLANT and Aerocat R-40, two typical examples of manned airship concepts, were proposed by the Israeli company Atlas LTA and the Argentine company Aerovehicles, respectively [4–6]. However, the research on manned airships mostly stays in the conceptual design and experimental stage, and there are almost no manned airships that are really put into operation. The main reason is that the safety and reliability of manned airships need to be further developed and verified.

The complex thermal environment of the manned airship will cause the dramatic fluctuation of lifting gas pressure and temperature, which will affect the dynamic performance of the airship [7, 8]. In addition, it will make an enormous impact on the surface temperature distribution of the nacelle, and then affect the design of the environmental control system of the manned airship. Hence, it is extremely important to research the thermal performance of the manned airship in order to ensure its safety and stability of flight.

In the last decade, scholars have conducted numerous investigations of stratospheric airships [9–12]. Lv *et al.* [13] proposed a simplified thermal model of a stratospheric airship, which includes scattered radiation, infrared radiation, reflected radiation, direct solar radiation, and convective heat transfer. Liu *et al.* [14] compiled an analysis program based on the thermal model of the stratospheric airship with a photovoltaic array and verified it with experimental data. The simulation results show that solar radiation has a significant effect on the thermal performance of the airship. Shi *et al.* [15–17] employed the design of the DOC experiment, analyzing the effect of season, wind speed, latitude, airbag distribution, envelope emissivity, envelope absorptivity, and various sensitive factors of the photovoltaic batteries on the thermal behavior of airships. Meng *et al.* [5] analyzed the effects of different flight parameters on the thermal behavior of the airship for long-distance transport by coupling different modules including thermal energy, output power, and dynamics. Dai *et al.* [18, 19] investigated the effect of forced convection heat transfer and the thermal performance of solar array on helium gasbag, respectively.

The above studies show that the thermal performance of airships is closely related to its own structure and material, but also strongly influenced by the surrounding environment [20–22]. In particular, the effects of solar radiation cannot be ignored [23–25]. However, the studies are limited to stratospheric airships, the limitations or weaknesses of the above-mentioned literature

*e-mail: shihong@nuaa.edu.cn

Manuscript submitted 2022-06-01, revised 2022-09-03, initially accepted for publication 2022-09-11, published in October 2022.

refer mainly to the following: (1) The difference in altitude between high-altitude airships and manned airships implies that they are subject to completely different environments; (2) the nacelle, as a manned structure, is subject to the vagaries of the environment during flight. Because it involves the safety of the crew, its thermal performance is even more important to the safety of the airship, and (3) some results have been obtained from previous thermal analyses, but there are no further analyses and practical applications of research in manned airships. This paper aims to make some efforts to do the above.

In this paper, the manned airship with an additional helium gasbag is taken as the research object. After establishing the thermal balance equations of each part of the airship, the numerical simulation analysis is carried out based on the C++ program and the thermodynamic performance of a manned airship is obtained. In addition, this paper focuses on the effects of influencing factors such as season, latitude, and airship orientation on the thermal behavior of manned airships. The results of this paper are beneficial for the design of thermal performance of future manned airships.

2. PHYSICAL AND MATHEMATICAL MODELING

2.1. Physical model

Based on the CA-120 airship, the structure of the manned airship in this paper is shown in Fig. 1. In order to maintain a stable flight altitude, the balance of the internal and external pressure is controlled by the charge and discharge of the helium bag. The design parameters for the envelope and the solar array are shown in Table 1.

Table 1
Design parameters of manned airships

Design parameters	Numerical value	Design parameters	Numerical value
Airship length	48 m	Envelope density	0.35 kg/m^3
Maximum diameter of airship	11.8 m	flight altitude	3 km
Volume of the gasbag	3500 m^3	Long wave radiation emissivity of envelope	0.6
Surface area of the airship	1446.75 m^2	Solar radiation absorption rate of envelope	0.38
Mass of the main helium gasbag	300 kg	Envelope transmittance	0.3
Mass of the additional helium gasbag	324.15 kg	Manned airship orientation	East
Mass of the keel and the nacelle	2558.85 kg	Wind speed	8 m/s

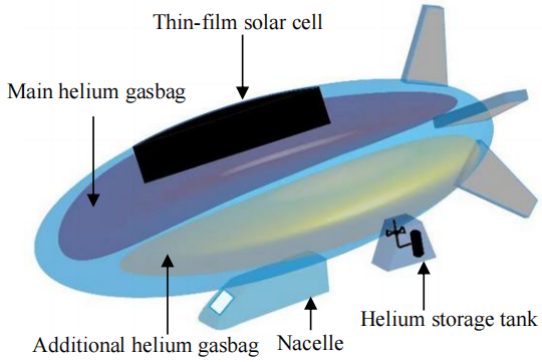

Fig. 1. Structure model of manned airship

2.2. Thermal environment

During the operation of the manned airship, the thermal environment is variable and complicated. Specifically, the thermal behavior of manned airships mainly includes the following aspects: (1) Radiation heat transfer is the main heat transfer process of manned airships, which includes short-wave radiation (direct, scattered, and reflected solar radiation) and long-wave radiation (ground, sky, and long-wave radiation inside and outside the envelope); (2) convective heat transfer includes external forced convective heat transfer and internal natural convective heat transfer. Among them, the internal natural convection heat transfer process comes from two closed spaces, namely inside the capsule and inside the nacelle, and (3) heat conduction is mainly the heat conduction between the envelope and the thin film solar cell. Because the envelope is quite thin, the heat conduction in its thickness direction can be neglected. The heat exchange mechanism is shown in Fig. 2.

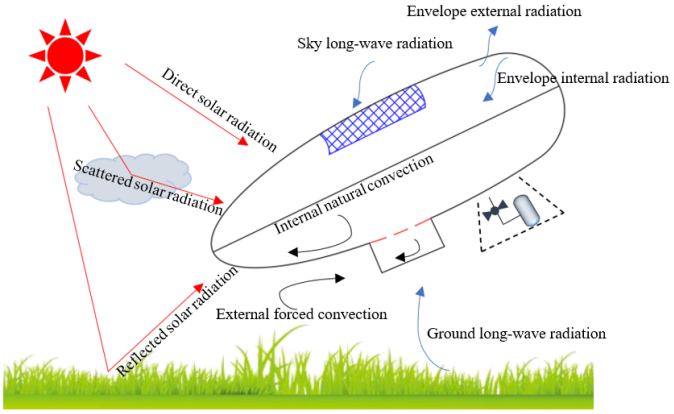

Fig. 2. Heat exchange mechanism of the manned airship

2.3. Heat balance equations

2.3.1. Solar radiation model

Solar radiation heat is one of the main heat sources for manned airships. Therefore, it is necessary to establish an accurate model of solar radiation. The solar radiation absorbed by the airship includes direct solar radiation I_{direct}, scattered solar radiation I_{scatter} and solar radiation reflected from the ground I_{reflect}. Before the solar radiation can be modelled, the spatial position of the sun must be determined.

As shown in Fig. 3, the spatial position of the sun is determined by the solar altitude angle α_{sun} and the solar azimuth angle γ_{sun}.

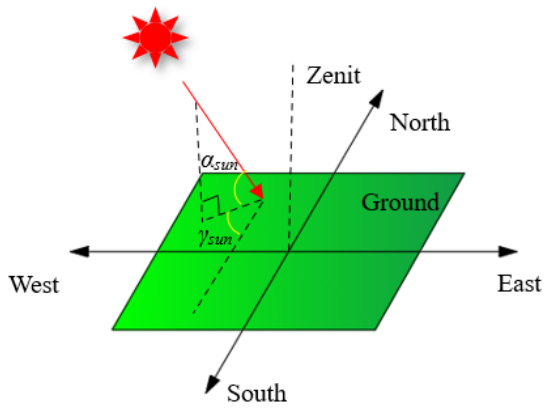

Fig. 3. The position of the sun relative to the ground

The solar altitude angle and the solar azimuth angle are expressed by equations (1) and (2):

$$\alpha_{\text{sun}} = \arcsin\left(\sin L \sin\delta + \cos L \cos\delta \cos\omega\right), \tag{1}$$

$$\gamma_{\text{sun}} = \arccos\left(\frac{\sin\alpha_{\text{sun}} \sin L - \sin\delta}{\cos\alpha_{\text{sun}} \cos L}\right), \tag{2}$$

where L, δ and ω are the latitude, the solar declination, and hour angle.

The solar declination angle δ and hour angle ω are shown in Fig. 4 and are represented by equations (3) and (4), respectively:

$$\begin{aligned}\delta = {} & 0.006322 - 0.405748\cos\left(\frac{2\pi}{366}N + 0.153231\right) \\ & + 0.00588\cos\left(\frac{4\pi}{366}N + 0.207009\right) \\ & + 0.003223\cos\left(\frac{6\pi}{366}N + 0.620129\right),\end{aligned} \tag{3}$$

$$\omega = (TH - 12)\cdot 15, \tag{4}$$

where N means the day being counted is the N-th day of the year, and January 1 is the first day of the year. TH is the solar time.

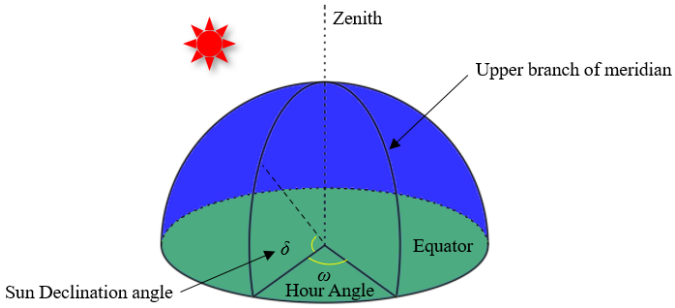

Fig. 4. The solar declination δ and hour angle ω

1. Direct solar radiation I_{direct} is defined by equation (5)

$$I_{\text{direct}} = \tau^{\frac{1}{\sin\alpha_{\text{sun}}}} I_0, \tag{5}$$

where τ is the transparency of the atmosphere. I_0 is the solar constant, and its average value for each month is shown in Table 2.

Table 2
Monthly mean solar radiation flux [10]

Months	1	2	3	4	5	6
I_0 (W/m^2)	1405	1394	1378	1353	1334	1316
Months	7	8	9	10	11	12
I_0 (W/m^2)	1308	1315	1330	1350	1372	1392

2. The scattered solar radiation I_{scatter} is defined by equation (6)

$$I_{\text{scatter}} = 0.5 I_0 \sin\alpha_{\text{sun}} \frac{1 - \tau^{\frac{1}{\sin\alpha_{\text{sun}}}}}{1 - 1.4\ln\tau}, \tag{6}$$

3. The solar radiation reflected from the ground I_{reflect} is defined by equation (7).

$$I_{\text{reflect}} = A_E\left(I_{\text{direct}} \sin\alpha_{\text{sun}} - I_{\text{scatter}}\right), \tag{7}$$

where A_E is the reflectance of the ground.

2.3.2. Thermodynamic model

Based on the analysis of the thermal environment for the manned airship, the thermal balance equations are established for six parts of the manned airship: the main helium gasbag, additional helium gasbag, the nacelle, the thin-film solar cell, the envelope under the solar cell and the other envelope cells.

The thermal balance equation of the main helium gasbag is:

$$m_1 c_1 \frac{\mathrm{d}T_1}{\mathrm{d}t} = -\sum Q_{e,1} + Q_{1,2} - P_1 \frac{\mathrm{d}V_1}{\mathrm{d}t}, \tag{8}$$

where m, c, T, V, P and t represent the mass, the specific heat capacity, the temperature, the volume, the pressure, and the flight time, respectively. Q is the heat exchange. Subscript e denotes a certain envelope cell. Subscript 1 denotes the main helium gasbag. Subscript 2 denotes an additional helium gasbag, where $Q_{e,1}$ and $Q_{1,2}$ are defined by equations (9) and (10):

$$Q_{e,1} = A_{e,1} h_{e,1}\left(T_1 - T_e\right), \tag{9}$$

$$Q_{1,2} = A_{1,2}\left(T_2 - T_2\right) \Big/ \left(\frac{1}{h_{e,1}} + \frac{x}{\lambda} + \frac{1}{h_{e,2}}\right), \tag{10}$$

where A, h, x, and λ represent the contact area, the convection heat transfer coefficient, thickness, and thermal conductivity, respectively.

The thermal balance equation of the additional helium gasbag is:

$$m_2 c_2 \frac{\mathrm{d}T_2}{\mathrm{d}t} = -\sum Q_{e,2} + Q_{2,1} + R_{g,\text{He}} T_2 \frac{\mathrm{d}m_2}{\mathrm{d}t} - P_2 \frac{\mathrm{d}V_2}{\mathrm{d}t}, \tag{11}$$

where $R_{g,\mathrm{He}}T_2\dfrac{\mathrm{d}m_2}{\mathrm{d}t}$ and R_g are the mass changes during the inflating and exhaust of additional helium gasbag and the gas constant. $Q_{e,2}$ is calculated in the same way as in equation (9) $Q_{1,2} = -Q_{2,1}$.

The thermal balance equation of the air in the nacelle is:

$$m_3 c_3 \frac{\mathrm{d}T_3}{\mathrm{d}t} = -\sum Q_{e,3}\,, \tag{12}$$

where subscript 3 denotes the nacelle.

The thermal balance equation of the thin-film solar cell is:

$$\begin{aligned}\dot{m}_i c_i \frac{\mathrm{d}T_i}{\mathrm{d}t} &= q_{\mathrm{direct},i} + q_{\mathrm{scatter},i} + q_{\mathrm{reflect},i} + q_{\mathrm{sky},i} \\ &+ q_{\mathrm{ground},i} - q_p - q_{i,a} - q_{i,j} - q_i\,,\end{aligned} \tag{13}$$

where q is the heat flow density. $\dot{m}$ is the mass per unit area. Subscript direct, scatter, reflect, sky, ground, p, and a are the direct solar radiation, the scattered solar radiation, the ground reflected solar radiation, the long wave radiation from the sky, the long wave radiation from the ground, output power, and external environment.

1) $q_{\mathrm{direct},i}$ is expressed by equation (14):

$$q_{\mathrm{direct},i} = \begin{cases} \alpha I_{\mathrm{direct}} \cos(\pi - \theta_i) & \theta_i \in \left(\dfrac{\pi}{2}, \pi\right], \\ 0 & \theta_i \in \left(0, \dfrac{\pi}{2}\right], \end{cases} \tag{14}$$

where α and θ_i are the solar radiation absorptivity and the angle between the external normal of solar thin film cell and the direction of direct solar radiation.

2) $q_{\mathrm{scatter},i}$ is expressed by equation (15):

$$q_{\mathrm{scatter},i} = \alpha I_{\mathrm{scatter}} X_{\mathrm{sky},i}\,, \tag{15}$$

where $X_{\mathrm{sky},i}$ is the sky angle coefficient.

3) $q_{\mathrm{reflect},i}$ is expressed by equation (16):

$$q_{\mathrm{reflect},i} = \alpha I_{\mathrm{reflect}} X_{\mathrm{sky},i}\,, \tag{16}$$

4) $q_{\mathrm{sky},i}$ is expressed by equation (17):

$$q_{\mathrm{sky},i} = \alpha_e \varepsilon_{\mathrm{sky}} \sigma T_{bb}^4 X_{\mathrm{sky},i}\,, \tag{17}$$

where α_e and σ are the absorption rate of long-wave radiation and the Stefan–Boltzmann constant, $\sigma = 5.67 \times 10^{-8}$ W/(m$^2\cdot$ K^4). $\varepsilon_{\mathrm{sky}}$ is the sky long-wave radiation emissivity. T_{bb} is the blackbody temperature.

5) $q_{\mathrm{ground},i}$ is expressed by equation (18):

$$q_{\mathrm{ground},i} = \alpha_e \varepsilon_{\mathrm{ground}} \sigma T_{\mathrm{ground}}^4 X_{\mathrm{ground},i} \eta\,, \tag{18}$$

where $\varepsilon_{\mathrm{ground}}$ is the ground-based longwave radiation emissivity. $X_{\mathrm{ground},i}$ is the ground angle coefficient. η is the transmittance.

6) $q_{i,a}$ is expressed by equation (19):

$$q_{i,a} = h_{i,a}\,(T_i - T_a)\,, \tag{19}$$

7) $q_{i,j}$ is expressed by equation (20):

$$q_{i,j} = \Delta T_{i,j}/R_{i,j}\,, \tag{20}$$

where $\Delta T_{i,j}$ is the temperature difference between the thin film solar cell and the envelope cell. $R_{i,j}$ is the thermal resistance between the thin film solar cell and the envelope cells.

8) q_i is expressed by equation (21):

$$q_i = \varepsilon \sigma T_i^4\,, \tag{21}$$

where ε is the grey scale of the thin-film solar cell.

The thermal balance equation of the envelope cells under the solar cell is:

$$\dot{m}_j c_i \frac{\mathrm{d}T_j}{\mathrm{d}t} = q_{i,j} - q_{j,1}\,, \tag{22}$$

$q_{j,1}$ is expressed by equation (23):

$$q_{j,1} = h_{j,1}\,(T_j - T_1)\,. \tag{23}$$

The thermal balance equation of the other envelope cells is:

$$\begin{aligned}\dot{m}_k c_k \frac{\mathrm{d}T_k}{\mathrm{d}t} &= q_{\mathrm{direct},k} + q_{\mathrm{scatter},k} + q_{\mathrm{reflect},k} + q_{\mathrm{sky},k} \\ &+ q_{\mathrm{ground},k} - q_k - q_{k,a} - q_{k,2}\,,\end{aligned} \tag{24}$$

where subscript k is a certain envelope cell other than a particular envelope cell under the thin-film solar cell.

2.4. Simulation methodology

The simulation methodology in this paper is shown in Fig. 5.

3. THEORETICAL MODEL VALIDATIONS

This paper verifies the reliability of the program based on the results of an airship (35 m) experiment with additional thin-film solar cells given by Harada *et al.* [26] and the results of the thermal model calculations of the airship by Xing *et al.* [27] The specific comparison diagram is shown in Fig. 6.

Figure 5 shows that the experimental data fluctuates greatly, and the calculated results of the program are relatively smooth, but the overall trend of simulation results shows good agreement with the experimental results. Specifically, the experimental calculation results fluctuate greatly before noon. The main reason is that the environmental performance at that time fluctuates greatly, and the program calculation is a given constant value, without considering the instantaneous performance of the environment at that time. In addition, the results of the self-programmed program calculations in this paper compare almost identically with the simulation results of Xing *et al.* [27]. Therefore, the simulation results in this paper are a beneficial reference for the study of the thermal performance of the manned airship.

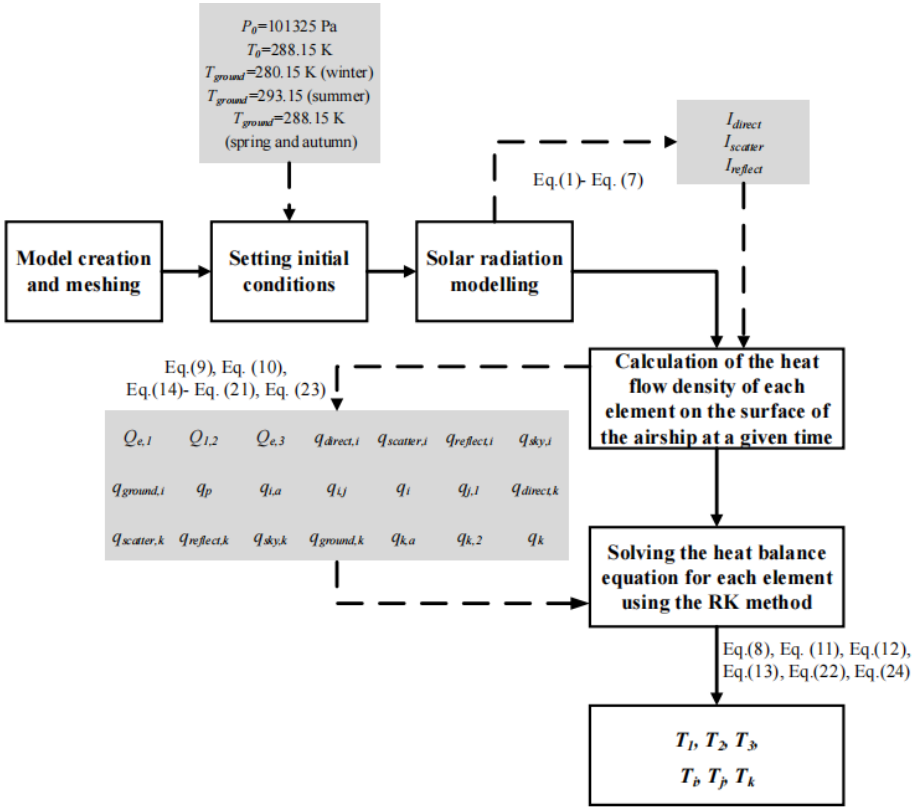

Fig. 5. The simulation methodology

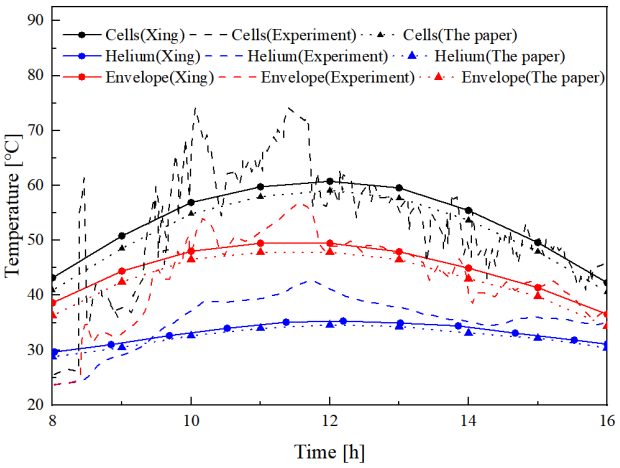

Fig. 6. Comparison of experimental data and calculated data

4. SIMULATION RESULTS AND ANALYSIS

According to the above model and design parameters, the temperature distribution of the manned airship and nacelle at the time of 0:00 a.m., 8 a.m., and 12:00 noon are shown in Figs. 7–9.

Figure 7 shows that the overall temperature of the manned airship at 0:00 a.m. is exceptionally low. The main reason for this phenomenon is the absence of solar radiation at night, so ground radiation plays a dominant role. The maximum temperature is at the bottom of the nacelle and can reach 286 K. The maximum temperature difference between the various parts of the airship is 13 K.

Figure 8 shows that the overall temperature of the manned airship rises at 8:00 a.m. when the sun rises. Because of the sunlight falling on the upper envelope of the airship, the temperature rise is most obvious on the upper envelope of the airship, especially in the solar cells. The maximum and minimum temperature of the manned airship is 300 K and 285 K, respectively. The minimum temperature is located in the lower envelope of airship. The maximum temperature difference between the various parts of the airship is 15 K. In summary, the temperature difference between the airship and the nacelle is not exceptionally large.

As can be seen in Fig. 9, the maximum temperature of the upper envelope is 322 K, which is significantly higher than the lower envelope. The temperature at the bottom of the nacelle is much higher than that of the rest of the nacelle owing to the influence of radiative heat transfer from the ground. The maximum temperature of the nacelle surface is 312 K. In addition, the maximum temperature difference in the nacelle can reach 29 K during the day, which has a significant impact on the environmental control system of the nacelle.

Figure 10 shows the variation of the average temperature of the manned airship with time.

As can be seen from Fig. 10, when the sun rises, the temperature of each part rises, but the temperature difference becomes larger and larger until midday. The temperature variation range of thin-film solar cells is greater than that of the upper envelope.

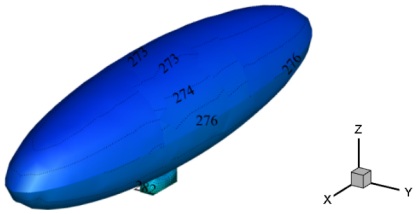

(a) Temperature distribution of the manned airship

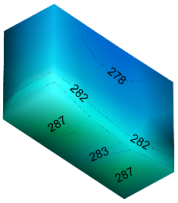

(b) Temperature distribution of nacelle

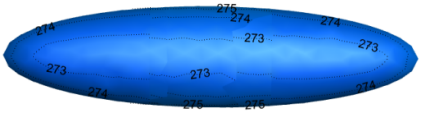

(c) Temperature distribution of the upper envelope of the manned airship

(d) Temperature distribution of the lower envelope of the manned airship

Fig. 7. Temperature distribution of the manned airship at 0:00 a.m.

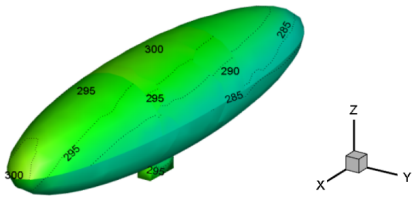

(a) Temperature distribution of the manned airship

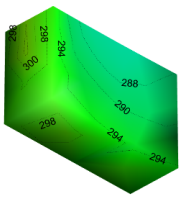

(b) Temperature distribution of nacelle

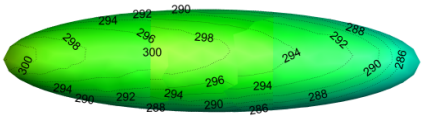

(c) Temperature distribution of the upper envelope of the manned airship

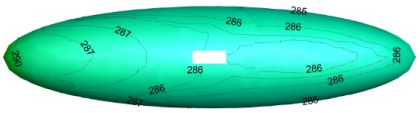

(d) Temperature distribution of the lower envelope of the manned airship

Fig. 8. Temperature distribution of the manned airship at 8:00 a.m.

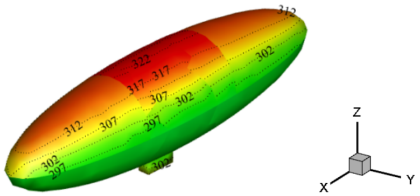

(a) Temperature distribution of the manned airship

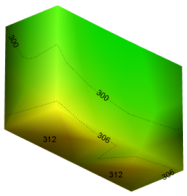

(b) Temperature distribution of nacelle

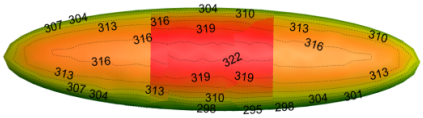

(c) Temperature distribution of the upper envelope of the manned airship

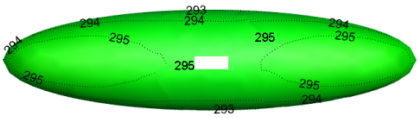

(d) Temperature distribution of the lower envelope of the manned airship

Fig. 9. Temperature distribution of the manned airship at 12:00 noon

The above phenomenon occurs because the thin-film solar cells receive more solar radiation at noon and are more affected by solar radiation. The average temperature variation of the solar cell is up to 40 K in one day, which is no lower than that of a traditional stratospheric airship. The temperature difference of the outer surface of the nacelle is 25 K, and the temperature difference of the envelope under the airship is about 16 K.

Figure 11 shows the temperature variation of the internal gas in a day.

As is shown in Fig. 11, the helium temperature inside the additional helium gasbag is similar to the air temperature inside the nacelle at night, both of which are higher than the helium temperature inside the main helium gasbag. The main reason for this is that at night, the ground temperature is higher than

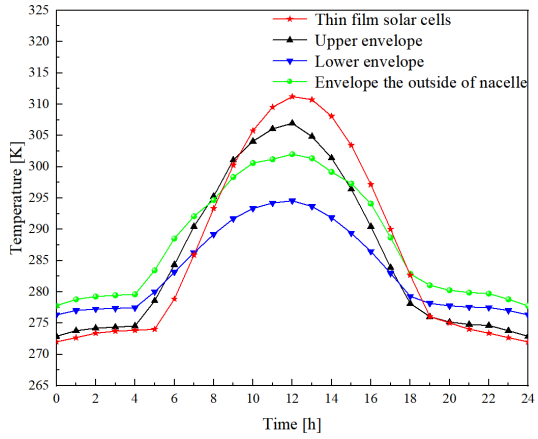

Fig. 10. Variation of the average temperature of the manned airship with time

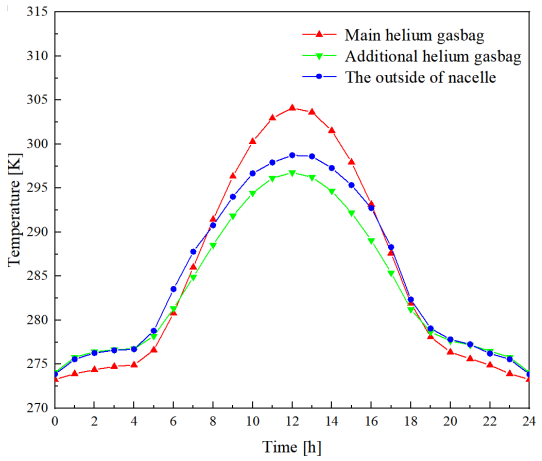

Fig. 11. Temperature variation of the internal gas with time

the gas, and the additional helium gasbag and the nacelle are influenced by the ground radiation relative to the main helium gasbag. Since the temperature of the main helium gasbag is mainly influenced by solar radiation, there is no solar radiation at night, and the temperature is almost constant between 8 p.m. and 4 a.m. As for helium, the temperature is lower than the atmospheric temperature, which is mainly due to the radiation behavior of the envelope with the sky (black ball model) at night, so the helium temperature will be lower than the atmospheric temperature. However, as the sun rises, the helium temperature inside the main helium gasbag exceeds the helium temperature inside the additional helium gasbag at about 7:00 a.m., then it exceeds the air temperature inside the nacelle at about 8:00 a.m. Significantly, without environmental control system, the air temperature in the nacelle changes dramatically during the day.

Furthermore, the air temperature inside the nacelle is always higher than the helium temperature inside the additional helium gasbag, which can be explained by the distinction of the gas mass. The helium gas will be charged and discharged into the high-pressure helium tank with temperature variation. Therefore, the helium mass in the additional helium gasbag is not fixed, and in this process, there is a huge heat and mass transfer.

5. INFLUENCING FACTORS ANALYSIS

5.1. Season

The thermal performance of a manned airship will experience the change of seasons during its service. Therefore, four typical days of the vernal equinox, summer solstice, autumn equinox, and winter solstice are selected as the research objects in this section respectively, and the thermal behavior of manned airships in different seasons is analyzed. Figure 12 shows the temperature distribution of manned airships in different seasons.

According to Fig. 12, the maximum temperatures of the manned airship in different seasons all deviate to the negative direction of the Y-axis at noon. The manned airship works at a latitude of 32 °N and the sun is always to the south of the manned airship. Correspondingly, the temperature distribution of the nacelle in the vernal equinox and autumn equinox are similar, and the maximum temperature between 306 K and 309 K is located on the south side of the nacelle. The maximum temperature of the nacelle in winter solstice is between

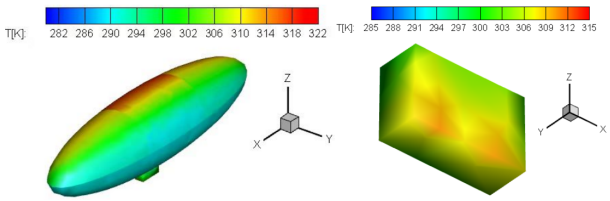

(a) Temperature distribution of the manned airship and nacelle in the vernal equinox

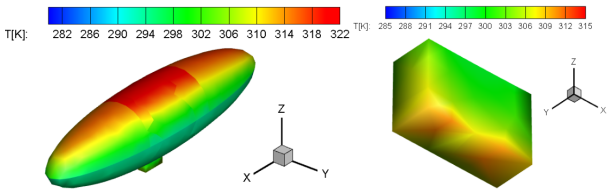

(b) Temperature distribution of the manned airship and nacelle in the summer solstice

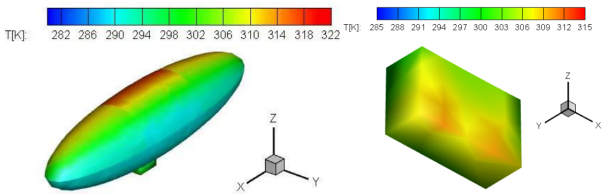

(c) Temperature distribution of the manned airship and nacelle in the autumn equinox

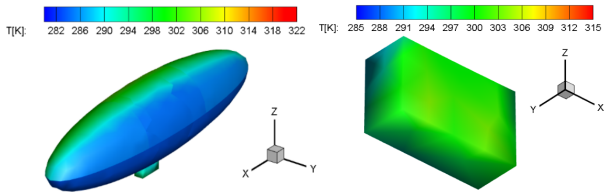

(d) Temperature distribution of the manned airship and nacelle in the winter solstice

Fig. 12. Temperature distribution of the manned airship at 12:00 noon in different seasons

300 K and 303 K located on the south side of the nacelle. The maximum temperature of the nacelle at the summer solstice is between 309 K and 315 K located at the bottom of the nacelle.

Figure 13 presents the temperature variation of each part of the manned airship in a day.

As is shown in Fig. 13, the temperature of various parts of the manned airship is similar during the vernal equinox and autumn equinox. The maximum and minimum temperature of the manned airship appears during the summer solstice and winter solstice, respectively. In addition, the temperature difference of solar cell, envelope, main, and additional helium gasbag is the largest at noon and amounts to 38.436 K, 25.244 K, 32.7 K, and 22.937 K, respectively.

In addition, the surface temperature of the cabin reaches its maximum at noon in all seasons. Its maximum temperature is around 299 K at the equinox, summer solstice, and autumn equinox. The main reason is that the ground surface temperature is similar during the vernal equinox, summer solstice, and autumn equinox. The maximum temperature of the nacelle in winter solstice is the smallest compared with other seasons, mainly because the surface temperature in winter solstice is lower, which is about 13 K lower than that in the summer solstice.

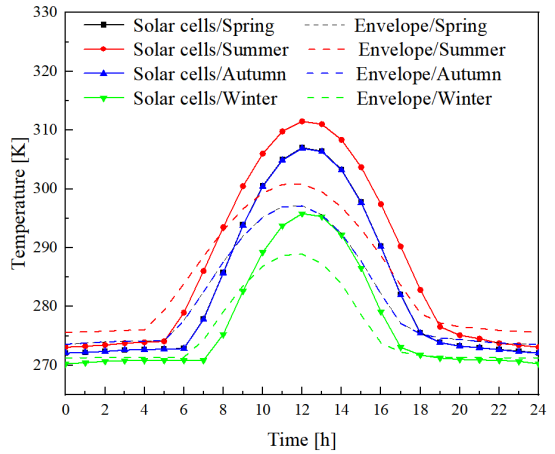

(a) solar cells

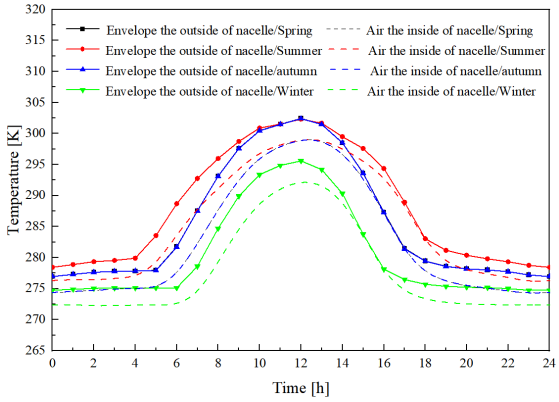

(b) nacelle

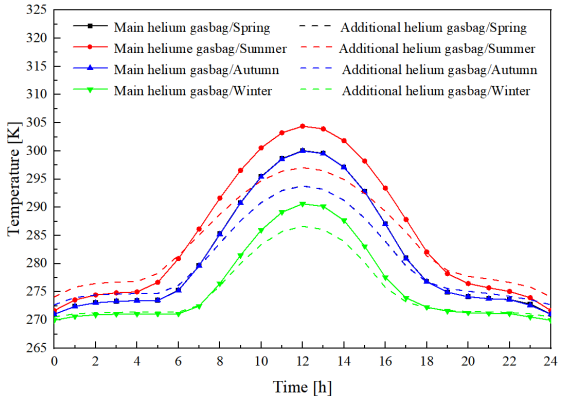

(c) helium gasbags

Fig. 13. Temperature distribution of the manned airship at 12:00 noon in different seasons

5.2. Latitude

The latitude variation means a difference in the solar zenith angle, and the solar radiation flux changes accordingly. Therefore, the influencing factor of latitude cannot be ignored in thermal prediction. Figure 14 shows the average temperature of the envelope, helium gas, and solar cells at three different latitudes. The average temperature of the nacelle at three different latitudes is shown in Fig. 15.

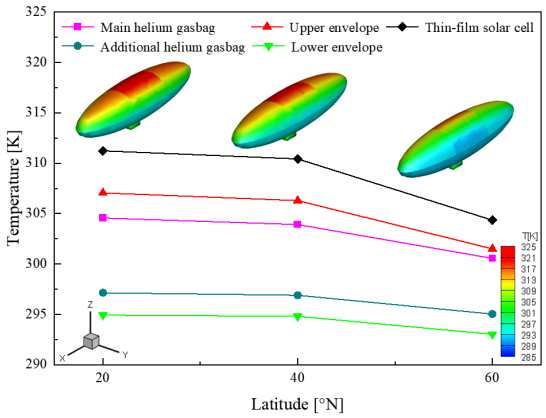

Fig. 14. Temperature variations of the airship at different latitudes

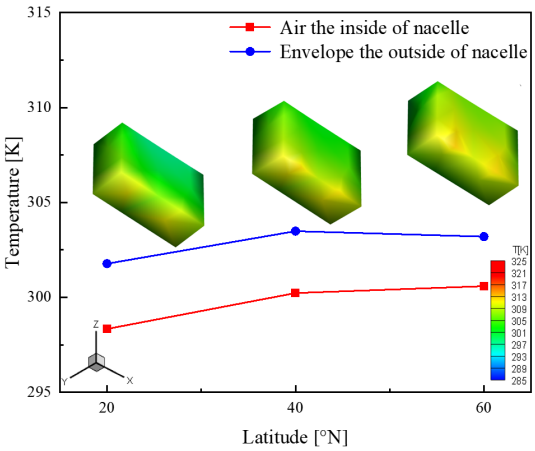

Fig. 15. Temperature variation of the airship nacelle at different latitudes

From Figs. 14 and 15, the average temperature on the envelope of the manned airship is more affected by latitude than that of the airship nacelle. The higher the latitude, the higher the average temperature of the internal gas and the envelope of the manned airship. From the temperature distribution, the lower parts of the manned airship are less affected by latitude, especially the nacelle. The main reason can be that the lower parts of the manned airship are less affected by solar radiation.

5.3. Orientation

In order to clearly observe the temperature distribution on the surface of the manned airship in different orientations, the temperature distribution of the head of the manned airship facing due east, north-east, and south-east at 8:00 a.m., 12:00 noon, and 4:00 p.m. is shown in Figs. 16–18, where the positive direction of the X-axis is east, and the positive direction of the Y-axis is north.

From Figs. 16–18, it can be seen that at 8:00 a.m. the temperature is higher in the positive direction of the X-axis of the manned airship, at noon the maximum temperature of the manned airship shifts to the upper part of the hull, and at 4:00 p.m. the maximum temperatures are concentrated in the negative direction of the X-axis. In summary, the maximum temperatures in the manned airship are determined by the solar altitude angle.

Figure 19 shows the temperature trends of helium, solar cells, envelope, and nacelle over one day for three operating conditions with the head facing due east, southeast, and northeast, respectively.

As can be seen from Fig. 19, the nighttime temperatures of the various parts of the manned airship are nearly identical for different orientations, and there are certain differences in temperature during the daytime except around midday, with the maximum temperature difference not exceeding 2 K. This is mainly because, with a higher solar altitude angle around midday, the sunward and backward sides of the manned airship are almost equally distributed, while the rest of the day, with a lower solar altitude angle, the sunward and backward sides are distributed differently.

However, the temperature distribution in the nacelle is not quite the same as in the other parts. During the night, the temperature inside and outside the nacelle does not change with orientation. During the day, however, the temperature inside and outside the nacelle is highest before midday in the southeast direction and after midday in the northeast direction due to the influence of ground radiation.

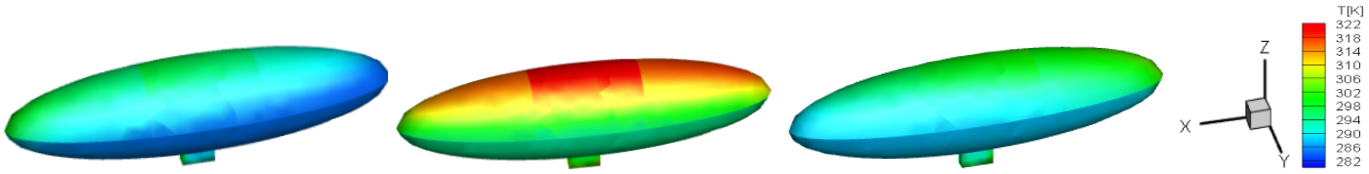

(a) 8:00 a.m. (b) 12:00 noon (c) 4:00 p.m.

Fig. 16. Temperature distribution of the manned airship due east

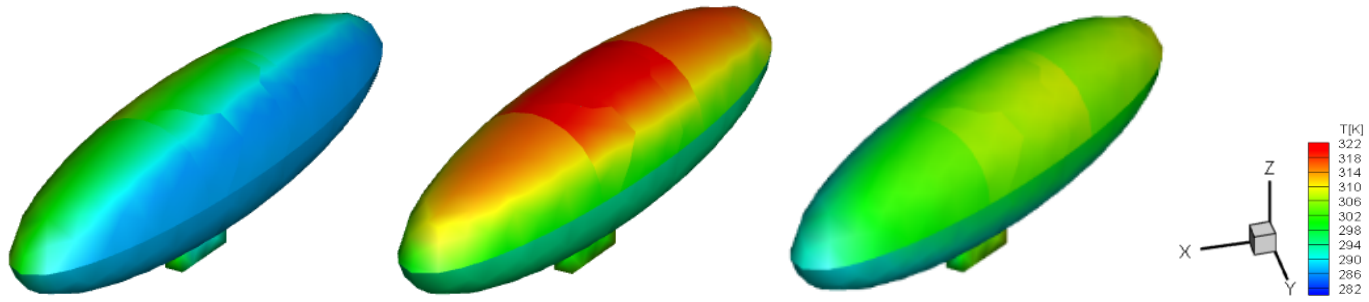

(a) 8:00 a.m. (b) 12:00 noon (c) 4:00 p.m.

Fig. 17. Temperature distribution of the manned airship in northeast orientation

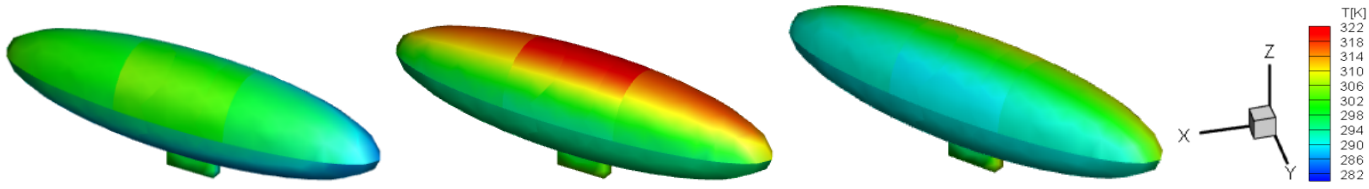

(a) 8:00 a.m. (b) 12:00 noon (c) 4:00 p.m.

Fig. 18. Temperature distribution of the manned airship in southeast orientation

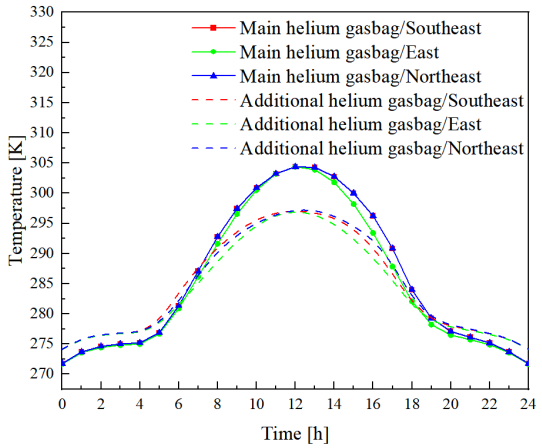

(a) Helium gasbags

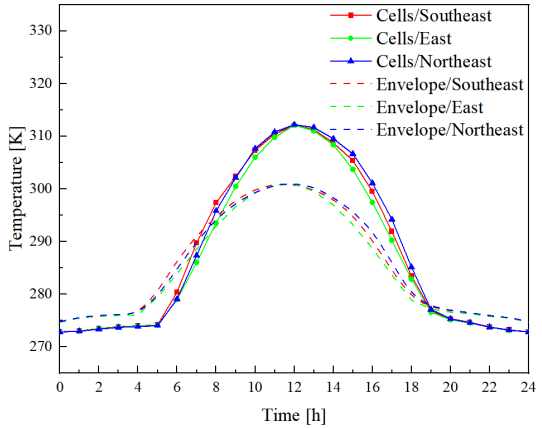

(b) Solar cell and envelope

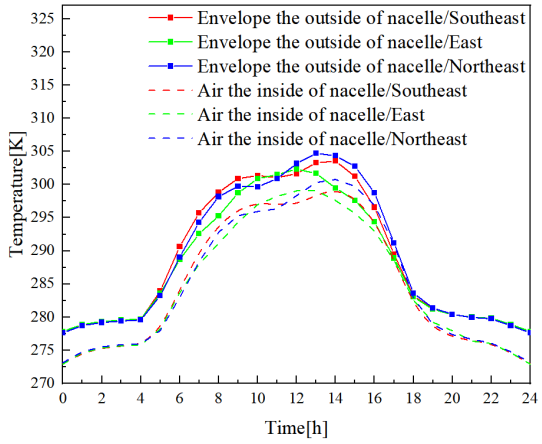

(c) Nacelle

Fig. 19. Temperature variation of the manned airship and nacelle with time under three different orientations

6. CONCLUSION

In this paper, the thermodynamic performance of the manned airship is analyzed, its thermal equilibrium equations are established, and the temperature performance of the manned airship is obtained by means of the C++ programming language. On the basis above, the effects of season, latitude, and orientation on the thermal performance of the manned airship are focused on, especially the nacelle. The following conclusions are obtained in this study.

- The maximum temperature difference between all parts of the manned airship at the same time can reach 29 K. The average temperature of the solar cells varies the most during the day, up to 40 K. The average temperature difference between the external walls of the nacelle varies by 25 K during the day. The results of the study show that the thermal load on the external walls of the nacelle varies greatly, not only in various locations at the same time but also in the same location at different times.
- The maximum envelope temperature of the manned airship in different seasons is oriented due south. The temperature distribution in the nacelle is similar in spring and autumn, with maximum temperatures between 306 K and 309 K, located on the southern side of the nacelle. The maximum envelope temperature in the nacelle ranges from 300 K to 303 K in winter and 309 K to 315 K in summer. The position of the maximum envelope temperature in the manned airship is determined by the solar radiation flux and solar altitude angle, while the position of the maximum envelope temperature in the nacelle is mainly determined by ground radiation.
- When the flight latitude of the manned airship changes from 20°N to 60°N, the upper part of the airship (solar cells, upper envelope, and main helium bladder) is strongly influenced by the latitude. The average temperature of the nacelle walls and internal gases is less affected by latitude and varies by about 1 K. However, the temperature distribution on the outer surfaces of the nacelle varies considerably, with the increase in latitude shifting the high-temperature zone from the bottom to the sides.
- The temperature distribution of the upper envelope of the airship varies considerably with orientation. However, the average temperature of the airship and the nacelle is less affected by orientation, while the maximum temperature difference does not exceed 2 K.

ACKNOWLEDGEMENTS

This research was supported by the Research Fund of Key Laboratory of Aircraft Environment Control and Life Support, MIIT, Nanjing University of Aeronautics and Astronautics (Grant No. KLAECLS-E-202001).

REFERENCES

[1] B.E. Prentice and R. Knotts, "Cargo airships: international competition," *J. Transp. Technol.*, vol. 4, no. 3, pp. 187–195, 2014, doi: 10.4236/jtts.2014.43019.

[2] A. Ceruti and P. Marzocca, "Conceptual approach to unconventional airship design and synthesis," *J. Aerosp. Eng.*, vol. 27, no. 6, pp. 04014035.1–04014035.14, 2014, doi: 10.1061/(ASCE)AS.1943-5525.0000344.

[3] J. Meng, M. Li, L. Zhang, and M. Lv, "Effect of flight parameters on thermal performance of a hybrid air vehicle for cargo transportation," *Appl. Therm. Eng.*, vol. 168, p. 114807, 2019, doi: 10.1016/j.applthermaleng.2019.114807.

[4] M. Manikandan and R.S. Pant, "Research and advancements in hybrid airships – A review," *Prog. Aerosp. Sci.*, vol. 127, p. 100741, 2021, doi: 10.1016/j.paerosci.2021.100741.

[5] J. Meng, M. Li, N. Ma, and L. Liu, "Multidisciplinary design optimization of a lift-type hybrid airship," *J. Beijing Univ. Aeronaut. Astronaut.*, vol. 47, no. 1, pp. 72–83, 2021, doi: 10.13700/j.bh.1001-5965.2020.0012.

[6] M. Manikandan and R.S. Pant, "Conceptual design optimization of high-altitude airship having a tri-lobed envelope," *Adv. Multidiscip. Anal. Optim.*, pp. 49–61, 2020, doi: 10.1007/978-981-15-5432-2_4.

[7] C. Stockbridge, A. Ceruti, and P. Marzocca, "Airship research and development in the areas of design, structures, dynamics and energy systems," *Int. J. Aeronaut. Space Sci.*, vol. 13, no. 2, pp. 170–187, 2012, doi: 10.5139/IJASS.2012.13.2.170.

[8] J. Wang, C. Li, and X. Meng, "A general calculation method to specify center-of-buoyancy for the stratospheric airship with multiple gas cells," *Adv. Space Res.*, vol. 67, no. 8, pp. 2517–2533, 2021, doi: 10.1016/j.asr.2021.01.014.

[9] L. Knap, C. Graczykowski, H. Szulc, and Z. Wolejsza, "Strategies for reduction of energy consumption during ascending and descending process of modern telescopic HAPS aerostats," *Bull. Pol. Acad. Sci. Tech. Sci.*, vol. 68, no. 1, pp. 155–168, 2016, doi: 10.24425/bpasts.2020.131833.

[10] J. Wang, X. Meng, C. Li, and W. Qiu, "Analysis of long-endurance station-keeping flight scenarios for stratospheric airships in the presence of thermal effects," *Adv. Space Res.*, vol. 67, no. 12, pp. 4121–4141, 2021, doi: 10.1016/j.asr.2021. 01.048.

[11] W. Yao, X. Lu, C. Wang, and R. Ma, "A heat transient model for the thermal behavior prediction of stratospheric airships," *Appl. Therm. Eng.*, vol. 70, no. 1, pp. 380–387, 2014, doi: 10.1016/j.applthermaleng.2014.05.050.

[12] H. Shi, B. Song, Q. Yao, and X. Cao, "Thermal performance of stratospheric airships during ascent and descent," *J. Thermophys Heat Transfer*, vol. 32, no. 4, pp. 816–821, 2009, doi: 10.2514/1.42634.M.

[13] M. Lv, Z. Yao, L. Zhang, H. Du, J. Meng, and J. Li, "Effects of solar array on the thermal performance of stratospheric airship," *Appl. Therm. Eng.*, vol. 124, pp. 22–33, 2017, doi: 10.1016/j.applthermaleng.2017.06.018.

[14] Q. Liu, Y, Yang, Y. Cui, and J. Cai, "Thermal performance of stratospheric airship with photovoltaic array," *Adv. Space Res.*, vol. 59, no. 6, pp. 1486–1501, 2017, doi: 10.1016/j.asr.2016.12.029.

[15] H. Shi, J. Chen, L. Hu, S. Geng, T. Zhang, and Y. Feng, "Multi-parameter sensitivity analysis on thermal characteristics of stratospheric airship," *Case Stud. Therm. Eng.*, vol, 25, p. 100902, 2021, doi: 10.1016/j.csite.2021.100902.

[16] H. Shi,; S. Geng, and X. Qian, "Thermodynamics analysis of a stratospheric airship with hovering capability," *Appl. Therm. Eng.*, vol. 146, p. 600–607, 2019, doi: 10.1016/j.applthermaleng.2018.10.034.

[17] H. Shi, J. Chen, S. Geng, T. Zhang, and X. Qian, "Envelope radiation characteristics of stratospheric airship," *Advances in Space Research*, vol. 68, pp. 600–607, 2021, doi: 10.1016/j.applthermaleng.2018.10.034.

[18] Q. Dai and X. Fang, "Numerical study of forced convective heat transfer around airships," *Adv. Space Res.*, vol. 57, no. 3, pp. 776–781, 2016, doi: 10.1016/j.asr.2015.11.031.

[19] Q. Dai, L. Cao, G. Zhang, and X. Fang, "Thermal performance analysis of solar array for solar powered stratospheric airship," *Appl. Therm. Eng.*, vol. 171, p. 115077, 2020, doi: 10.1016/j.applthermaleng.2020.115077.

[20] H. Zhang, X. Fang, Y. Wang, and L. Zhang, "Effect of vapor condensation on ascending performance of stratospheric airship," *Adv. Space Res.*, vol. 65, no. 8, pp. 2062–2071, 2020, doi: 10.1016/j.asr.2020.01.027.

[21] W. Zheng, X. Zhang, R. Ma, and Y. Li, "A Simplified Thermal Model and Comparison Analysis for a Stratospheric Lighter-Than-Air Vehicle," *J. Heat Transfer*, vol. 140, no. 2, p. 022801, 2019, doi: 10.1115/1.4037194.

[22] W. Zhu, Y. Xu, J. Li, H. Du, and L. Zhang, "Research on optimal solar array layout for near-space airship with thermal effect," *Solar Energy*, vol. 170, pp. 1–13, 2018, doi: 10.1016/j.solener.2018.05.023.

[23] J. Wang, X. Meng, and C. Li, "Recovery trajectory optimization of the solar-powered stratospheric airship for the station-keeping mission," *Acta Astronaut.*, vol. 178, pp. 159–177, 2021, doi: 10.1016/j.actaastro.2020.08.016.

[24] J. Li, M. Lv, D. Tan, W. Zhu, K. Sun, and Y. Zhang, "Output performance analyses of solar array on stratospheric airship with thermal effect," *Appl. Therm. Eng.*, vol. 104, pp. 743–750, 2016, doi: 10.1016/j.applthermaleng.2016.05.122.

[25] Y. Zhang, J. Li, M. Lv, D. Tan, W. Zhu, and K. Sun, "Simplified analytical model for investigating the output power of solar array on stratospheric airship," *Int. J. Aeronaut. Space Sci.*, vol. 17, no. 3, pp. 432–441, 2016, doi: 10.5139/IJASS.2016.17.3.432.

[26] K. Harada, K. Eguchi, M. Sano, and S. Sasa, "Experimental study of thermal modeling for stratospheric platform airship," *Aiaas Aviation Technology, Integration, & Operations*, 2003, doi: 10.1016/j.applthermaleng.2017.05.168.

[27] D. Xing, Q. Dai, and C. Liu, "Thermal characteristics and output power performances analysis of solar powered stratospheric airships," *Appl. Therm. Eng.*, vol. 123, pp. 770–781, 2017, doi: 10.1016/j.applthermaleng.2017.05.168.